

Blind Deconvolution with Non-local Sparsity Reweighting

Dilip Krishnan¹, Joan Bruna² and Rob Fergus^{2,3}

¹: CSAIL, Massachusetts Institute of Technology

²: Courant Institute, New York University, ³: Facebook Inc.

November 1, 2021

Abstract

Blind deconvolution has made significant progress in the past decade. Most successful algorithms are classified either as Variational or Maximum a-Posteriori (*MAP*). In spite of the superior theoretical justification of variational techniques, carefully constructed *MAP* algorithms have proven equally effective in practice. In this paper, we show that all successful *MAP* and variational algorithms share a common framework, relying on the following key principles: sparsity promotion in the gradient domain, l_2 regularization for kernel estimation, the use of convex (often quadratic) cost functions and multi-scale estimation. We also show that sparsity promotion of latent image gradients is an efficient regularizer for blur kernel estimation. Our observations lead to a unified understanding of the principles required for successful blind deconvolution. We incorporate these principles into a novel algorithm that has two new priors: one on the latent image and the other on the blur kernel. The resulting algorithm improves significantly upon the state of the art.

1 Introduction

Starting with the influential work of Fergus et al. [1], the state of the art in blind deconvolution has advanced significantly. For blurred images involving camera translations or rotations, impressive performance levels have been achieved by a number of algorithms [2, 3, 4, 5, 6, 7, 8, 9, 10].

The simplest form of the blind deconvolution problem arises from the following formation model:

$$y = x_0 \star k_0 + n \tag{1}$$

where y is the observed blurred and noisy image, x_0 the unknown sharp image and k_0 is the unknown blur kernel. The noise n is assumed IID Gaussian noise with unknown variance σ^2 . Blind deconvolution is the problem of recovering x_0 and k_0 , given only the observation y . The model in 1 assumes spatially uniform blur, and can be extended to non-stationary blurs due to in-plane rotations, as done in Whyte et al. [7]. If k_0 is known, then the problem reduces to that of non-blind deconvolution [11, 12].

Blind deconvolution is ill-posed since neither the sharp image x_0 , the blur kernel k_0 or the noise variance are known. To alleviate these issues, prior assumptions on the structure of x_0 and k_0 must be employed. A commonly used prior on x_0 is the heavy-tailed prior (Levin et al. [12]), motivated from the observation that gradients of natural images follow a hyper-Laplacian distribution. Using this prior leads to good results in many applications such as non-blind deconvolution [11], super-resolution [13] and transparency separation [14]. If $\nabla x = (\nabla x)_i$, the heavy-tailed distributions used are of the form $\mathbf{p}(x) = \prod_i p(\nabla x_i)$ with $p(z) \propto e^{-|z|^\alpha}$. The exponent α is typically in the range of 0.6 to 0.8 [12]. Priors on the kernel k_0 have received lesser attention, but they usually tend to work on the sparsity of the kernel for motion blurs, such as the l_1 norm $\|k\|_1$ (Shan et al. [15]), or sparsity of coefficients under a curvlet transform (Cai et al. [16]).

Unfortunately, using the above priors in a naive alternating minimization (AM) framework leads to the trivial solution $\hat{x}_0 = y, \hat{k}_0 = \delta$, where δ is the Dirac. In [17], Levin et al. analyze the reasons behind this phenomenon, when the heavy-tailed prior is used. The fundamental reason is quite simple: the probability of a sharp image x is lower under the commonly used heavy-tailed prior, with exponent in the range of 0.6-0.8. In their paper, Levin et al. also identified a workaround. The same authors, in a follow-up work [6] present a simplified version of the algorithm of Fergus et al. [1]. The paper [1] itself was based on the work of Miskin and MacKay [18]. We call this family of related algorithms the variational model.

A different family of algorithms such as those of [3, 2] are categorized as Maximum a-Posteriori (*MAP*). The chief distinction between the variational and *MAP* algorithms is the use of probability distributions in the former, as opposed to point estimates in the latter. The kernel estimate \hat{k}_0 is thus obtained by marginalizing the posterior distribution over all possible images x . This Bayesian approach is usually seen as a strong advantage for the variational methods since the uncertainty of an estimate is taken into account. Indeed, they perform well empirically. However, in practice, the marginalization is intractable and a series of approximations are per-

formed to realize a practical algorithm. *MAP* formulations, on the other hand, use alternating minimization (AM) updates on \hat{x}_0 and \hat{k}_0 , resulting in non-convex optimizations. In spite of this seemingly inferior formulation, in practice the best *MAP* formulation techniques have proven as effective as variational methods. The key to their performance is the use of additional steps to supplement the AM iterations.

We make the following contributions in this paper: we first show that the use of approximations in the variational method and non-naive approaches in *MAP* methods lead to essentially the same framework. We show theoretically and experimentally that sparsity inducing regularizations are the key ingredient, irrespective of whether they provide good image gradient priors or not. This helps explain why the top-performing methods all achieve similar performance. We develop a new algorithm based on our insights that achieves significantly better than state of the art results on the standard benchmark of [17]. Our algorithm has two novel priors. The first is a patch-based sparsity promotion prior on the latent image which estimates salient geometric features that are crucial for good kernel estimation. The second is a frequency-domain based kernel prior that performs adaptive regularization of the latent kernel to alleviate the aperture problem.

Our work has shared ground with that of Wipf and Zhang [10], who also seek to explain the reasons behind the success of the variational approach. We show that most successful algorithms (not just variational) follow similar principles. Our resulting recipes are conceptually simpler than that suggested by [10], and we also provide directions for future improvements.

The variational and *MAP* paradigms do not cover all deconvolution algorithms. For example, the spectral analysis based algorithm of Goldstein and Fattal [4] and the Radon transform based method of Lin et al. [19] are two examples where our current analysis does not hold. Nevertheless, we note that at present, these alternative methods do not perform at state of the art levels compared to the *MAP* and variational algorithms.

Notations: We denote by $\mathcal{F}(x)$ or x_f the Fourier transform of x . $\nabla x = (\partial_h x, \partial_v x)$ denotes the gradient of a two-dimensional signal.

2 Variational and *MAP* Approaches

In this section, we consider in detail the variational algorithm of Levin et al. [6] and Wipf and Zhang[10], and the *MAP* algorithms of Xu et al. [9], Xu and Jia [3] and Cho and Lee [2]. These algorithms are all considered state of the art, and perform very well on the benchmark dataset of Levin et al. [17].

All of the above algorithms work in the gradient domain for kernel estimation. Since convolution commutes with derivatives, this does not change the form of the cost function 1. The gradient space is used to determine a kernel \widehat{k}_0 , and the final sharp image \widehat{x}_0 is typically recovered with a non-blind deconvolution algorithm such as Krishnan and Fergus [11].

2.1 Naive MAP

The naive MAP algorithm that is prone to poor solutions solves the following cost function:

$$(\widehat{\nabla x}_0, \widehat{k}_0) = \arg \min_{\nabla x, k} \lambda \|\nabla y - \nabla x \star k\|^2 + \sum_i |\nabla x_i|^\alpha \quad (2)$$

Alternating minimization is usually employed: given a current estimate k_n , a new update ∇x_{n+1} is computed, and vice-versa. The regularizer on ∇x is a heavy tailed prior Levin et al. [17] with $\alpha < 1$. It has been shown in [17] that this cost function leads to the trivial solution $\widehat{x}_0 = y, \widehat{k}_0 = \delta$. This is because the trivial solution achieves the lowest cost for both the likelihood term $\|\nabla x \star k - \nabla y\|^2$ and the regularizing term $\sum_i |\nabla x_i|^\alpha$. 1 shows this phenomenon for the 32 blurred images from the dataset of [17] for values of $\alpha = 0.5$ and $\alpha = 0.8$. Heavy-tailed priors give a lower cost to the blurred image because the blurring operation reduces the overall gradient variance, which reduces $\sum_i |\nabla x_i|^\alpha$. On the other hand, because zero gradients near strong edges become non-zero due to blur, an opposite effect is that $\sum_i |\nabla x_i|^\alpha$ is increased by blurring. For $\alpha = 0.5$ or larger, the former effect dominates and this causes the measure to prefer the blurred image. It is shown in Wipf and Zhang [10], that for very small α values, the situation may be reversed. However, the resulting cost functions are numerically unstable and difficult to handle.

2.2 Successful MAP Methods

In Cho and Lee [2], alternating x and k updates are performed using the following equations:

$$\begin{aligned} x_{n+1} &= \arg \min_x \sum_j \|\partial_j x \star k_n - \partial_j y\|^2 + \alpha \|\partial_j x\|^2 \\ k_{n+1} &= \arg \min_k \sum_j \|\partial_j x_{n+1} \star k - \partial_j y\|^2 + \beta \|k\|^2, \end{aligned} \quad (3)$$

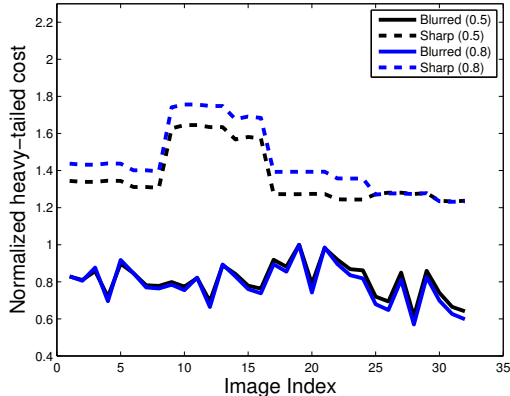


Figure 1: Comparison of costs of blurred and sharp images under heavy-tailed prior: 32 images from the dataset of Levin et al. [17] for $\alpha = 0.5$ and $\alpha = 0.8$. Gradients of blurred images have lower cost.

where j indexes a set of partial derivative filters; in their implementation [2] use 6 filters¹. Clearly, due to the phenomenon seen in 1, this simple formulation has little hope of succeeding since the quadratic regularization forces x_n towards the blurred image y . Therefore, Cho and Lee introduce an additional step to promote sparsity in $\{\partial_\gamma x\}$. This additional step is a shock filter Osher and Rudin [20], which suppresses gradients of small magnitude and boosts large magnitude gradients. This shock filtering step is performed after the x update step, and prior to the k estimation, thereby preventing a drift towards the trivial solution.

Xu and Jia [3] also use a shock filter, and additionally an importance map, which is designed to down weight the importance of low magnitude gradients as well as isolated spikes. The k update step is identical to that of Cho and Lee [2], and is given in 3, also using an l_2 (quadratic) norm on k .

The very recent work of Xu et al. [9] employs an ℓ_0 -like prior on ∇x . The cost functions that they solve to update x and k are given by:

$$\begin{aligned}
 x_{n+1} &= \arg \min_x \|y - x \star k_n\|^2 + \lambda \Phi(\nabla x) \\
 k_{n+1} &= \arg \min_k \|y - x_{n+1} \star k\|^2 + \gamma \|k\|^2,
 \end{aligned} \tag{4}$$

where Φ is a function that approximates $\|\nabla x\|_0$. The x update step involves a series of quadratic relaxations that progressively approximate the ℓ_0 function more closely,

¹The filters are first-order and second-order derivative filters in horizontal, vertical and diagonal directions.

thereby imposing sparsity on the gradients ∇x . The above papers, [2, 3, 9] and other *MAP* methods, periodically enforce non-negativity and sum-to-1 constraints of the entries of k . Generally, this is done after a k -update step.

2.3 Variational Methods

The variational method was introduced to blind deconvolution by Miskin and Mackay [18], who considered the blind deconvolution and separation of cartoon images. They imposed a highly sparsity promoting prior on x , given by a mixture of Laplacians.

Fergus et al. [1] extended the algorithm of Miskin and Mackay to natural images. The contribution of [1] was to realize that the gradient fields of natural images are generally highly sparse, and thereby working in gradient space allows the extension of the original algorithm of Miskin and Mackay.

A conceptually simpler version of the algorithm of [1] was given by Levin et al. [6]. While [1] is variational in both x and k , [6] is variational only in x . Under a probabilistic interpretation of blind deconvolution, the estimation of k is given by:

$$\hat{k} = \arg \max_k p(k|y) = \arg \max_k \int p(y|k, x)p(x)dx \quad (5)$$

However, 5 is computationally intractable, and variational approximations are introduced in [1, 6] to realize a practical algorithm. One can show [10, 6] that the final form of the resulting algorithm has the form

$$\begin{aligned} \nabla x_{n+1} &= \arg \min_x \frac{1}{\eta_n^2} \|\nabla y - x \star k_n\|^2 + \sum_i (w_{i,n} x)^2 \\ k_{n+1} &= \arg \min_k \|\nabla y - \nabla x_{n+1} \star k\|^2 + \lambda_n \|k\|^2, \end{aligned} \quad (6)$$

where η_n refers to a noise level parameter and the weights $w_{i,n}$ evolve dynamically to penalize current estimates $\nabla x_{i,n}$ of low gradient amplitudes and to “protect” large gradients. The resulting iterative minimization therefore favors a sparse ∇x_{n+1} . Note that in 6, we are estimating the latent image gradients. On the other hand, the k step consists of a ridge regression, where the parameter $\lambda_n = \text{Tr}(\Sigma_n^{-1})$ and Σ_n is a diagonal covariance of ∇x_n estimated from the previous x -step [6]. As a result, the regularization strength is a measure of the overall variance in the estimate of ∇x_{n+1} .

3 The Common Components

This section explains why sparsity promoting regularizations play a central role for blind deconvolution. We argue that the main reason is not related to the prior

distribution of image gradients.

3.1 Sparsity Promotion

The total variation has been extensively used as an efficient regularizer for several inverse problems [21, 22], including denoising and non-blind deconvolution. It corresponds to the ℓ_1 norm computed on image gradients ∇x , which is known Rudin et al. [22] to promote solutions whose gradients are sparse.

This suggests that a similar sparsity-promoting prior will also be useful for the blind-deconvolution inverse problem. For that purpose, several authors [15, 23] suggested using $\|\nabla x\|_p$ with $p \leq 1$ as a prior. Similarly, all variational approaches are based on sparsity promoting priors Wipf and Zhang [10]. Since the derivative is a linear, translation invariant operator, we have $\nabla y = (\nabla x_0) \star k_0 + \nabla n$. This results in a cost function of the form

$$\|\nabla y - x \star k\|^2 + \Phi(x) ,$$

where Φ is a sparsity-promoting function. Since natural images typically have a spectrum decaying as $\sim \omega^{-2}$ and $\mathcal{F}(\partial x)(\omega) = i\omega\mathcal{F}(x)(\omega)$, it results that the likelihood term expressed in the gradient domain is simply a reweighted ℓ_2 norm with equalized frequencies.

However, the blind deconvolution inverse problem requires not only the estimation of x_0 but also estimating the kernel k_0 . We argue that enforcing sparsity of ∇x is a regularizer for \widehat{k}_0 which is highly efficient, even when input images do not have sparse gradients.

We shall consider a ridge regression (l_2 norm) on the kernel. Let us concentrate on the case of spatially uniform blur of 1, and let us suppose the kernel k_0 has compact support of size S . The following proposition, proved in Appendix A, shows that if one is able to find an approximation of ∇x_0 which has small error in *some* neighborhood Ω of the image domain, then setting to zero ∇x outside Ω yields a good approximation of k_0 . We denote $dist(i, \Omega) = \inf\{|i - j|, j \in \Omega\}$.

Proposition 3.1 *Let $y = x_0 \star k_0 + n$, with $\sum_i k_{0i} = 1$. For a given x and a given neighborhood Ω , let*

$$\begin{aligned} \epsilon^2 &= \|x - x_0\|_{\Omega, S}^2 := \sum_{dist(i, \Omega) \leq S} |x_i - x_{0i}|^2 , \\ \gamma^2 &= \|x_0\|_{\Omega, S}^2 , \end{aligned} \tag{7}$$

and let us assume that the matrix A whose columns are

$$(A)_j = \{x_{0j-i}; |i| \leq S\}_{j \in \Omega}$$

satisfies $\lambda_{\min}^2(A) = \inf_{\sum_i y_i = 0, \|y\|=1} A(y) = \delta > 0$. Then, by setting

$$\tilde{x}_i = \begin{cases} x_i & \text{if } i \in \Omega, \\ 0 & \text{otherwise,} \end{cases} \quad (8)$$

the solution of

$$\hat{k}_0 = \arg \min_{k \text{ s.t. } \sum_i k_i = 1} \|y - \tilde{x} \star k\|^2 + \lambda \|k\|^2 \quad (9)$$

satisfies

$$\|\hat{k}_0 - k_0\| \leq C \|k_0\| + c, \quad (10)$$

where $C = O(\max(\epsilon\gamma\delta^{-1}, \lambda))$ and $c = O(\|n\|_{\Omega}\gamma\delta^{-1})$.

This proposition shows that in order to recover a good estimation of the kernel, it is sufficient to obtain a good estimation of the input gradients on a certain neighborhood Ω . Sharp geometric structures and isolated singularities are natural candidates to become part of Ω , since they can be estimated from y by thresholding the gradients. This partly explains the numerical success of shock filtering based methods such as those in Cho and Lee [2] and Xu and Jia [3].

Promoting sparsity of the image gradients thus appears to be an efficient mechanism to identify the support of isolated geometric features, rather than a prior for the distribution of image gradients. In particular, Proposition 3.1 shows that images having textured or oscillatory regions do not necessarily increase the approximation error, as long as they also contain geometric features. Proposition 3.1 gives a bound on the estimation error of k_0 given a local approximation of x_0 . The error is mainly controlled by ϵ , the approximation error of x_0 on the active set Ω , and δ , which depends upon the amount of diversity captured in the active set. The so-called *aperture problem* corresponds to the scenario $\delta = 0$, in which k_0 can be recovered only on the subspace spanned by the available input data.

Finally, let us highlight the connection between this result and the recent work of Ahmed et al. [24]: the authors show that under certain identifiability conditions, one can recover x_0 and k_0 by solving a convex program on the outer product space. In this sense, the sparsity enhancement of x helps identify a subspace Ω such that the restrictions $y|_{\Omega}, x|_{\Omega}$ satisfy better identifiability conditions.

3.2 ℓ_2 norm on k

The inverse problem of 1 requires regularisation not only for the unknown image but also for the unknown kernel. It is seen from 2 that all the top-performing methods use an ℓ_2 ridge regression on the kernel k , which regularises the pseudo inverse associated to

$$\min_k \|\nabla y - \nabla \hat{x} \star k\|^2 .$$

An ℓ_2 norm gives lower cost to a diffuse kernel, which helps to push away from the trivial solution $k = \delta$. Moreover, the previous section showed that the necessary sparse regularisation of the x -step may cause the regression to be ill-conditioned due to the aperture problem.

Since the ridge regression only contains Euclidean norms, one can express it in the Fourier domain

$$\min_k \|y_f - x_f \cdot \mathcal{F}(k)\|^2 + \lambda \|\mathcal{F}(k)\|^2 ,$$

where y_f and x_f are respectively the Fourier transforms of ∇y and $\widehat{\nabla x}$ computed at the resolution of the kernel. It results in the well-known Wiener filters, in which frequencies with low energy in the current estimate $\widehat{\nabla x}$ are attenuated by the ridge regression. This may create kernels with irregular spectra, which translates into slow spatial decay, thus producing diffused results. In order to compensate for this effect, some authors such as Levin et al. [6] introduced a sparsity-promoting term in the estimation of k as well. Since we assume positive kernels with constant DC gain (set to 1 for simplicity), $\|k\|_1 = 1$ by construction, thus requiring a regulariser of the form $\|k\|_p$ with $p < 1$ in practice.

3.3 Convex Sub-problems

A notable aspect of the successful algorithms is the use of quadratic cost functions for both the x and k sub-problems (even though the joint problem is non-convex). Quadratic cost functions are especially simple to optimize when convolutions are involved: fast FFT or Conjugate Gradient methods may be used. For non-quadratic convex cost functions, iteratively reweighed least squares Daubechies et al. [25] may be used.

When using a convex sparsity-promoting regularizer for ∇x , one may compromise the sparsity promotion ability. However, this must be balanced against the fact that for a non-convex regularizer, it can be hard to achieve a sparse enough solution, as seen in the results of Krishnan et al. [26], which uses a non convex regulariser.

The tradeoff between sparsity-promotion and the solvability of a regularizer is therefore an important design criterion. The re-weighted methods of Levin et al. [6] and Xu et al. [9] seem to strike a good balance by solving convex (quadratic) cost functions. In our experiments with the publicly released code of [6], we found that solving each sub-problem to a high level of accuracy was crucial to the performance of the method. For example, reducing the number of conjugate gradients iterations in the ∇x update of 6. caused the performance to be much poorer. This is due to the lack of sufficient level of sparsity in the resulting ∇x .

3.4 Multi-scale Framework

Due to the non-convex nature of the blind deconvolution problem, it is easy to get stuck at a local minimum. A standard mechanism to overcome this is to use a coarse-to-fine framework for estimating the kernel. This coarse-to-fine scheme is used by all successful algorithms. At each scale in the pyramid, the upsampled kernel from the coarser level, and the downsampled blurred image from the finest level are used as an initialization. At the coarsest level, a simple initialization away from the δ kernel is used, such as a 2-pixel horizontal or vertical blur.

4 Our New Algorithm

We combine the principles described above into a new algorithm that performs above the state of the art on the benchmark dataset of Levin et al. [17]. In addition to the high performance, an advantage of our method is that it has only two user-defined parameters that determine the regularization levels on the estimation of k . This is in contrast with methods such as [9, 2] which have a few parameters whose settings can be hard to estimate.

We work in derivative space, using horizontal and vertical derivative filters. As argued in section 3.1, our x update step is given by a reweighted least squares formulation which promotes solutions with isolated geometric structures, whereas the k update solves a least squares regression using ℓ_2 and ℓ_p regularisation discussed in 3.2. However, unlike in 3.2, we use a novel reweighted ℓ_2 prior on k (discussed below):

$$\begin{aligned} \nabla x_{n+1} &= \arg \min_x \|\nabla y - x \star k_n\|^2 + \sum_i w_{i,n} x_i^2, \\ k_{n+1} &= \arg \min_k \|\nabla y - \nabla x_{n+1} \star k\|^2 + \|Ak\|_2^2 + \lambda \|k\|_{0.5}. \end{aligned} \quad (11)$$

The weights $w_{i,n}$ at each iteration are based on the current estimate ∇x_n . They are designed to select the regions of ∇x_n with salient geometrical features while

attenuating the rest. Let $p_{i,n}$ be the patch of size R centered at pixel i of ∇x_n . We consider

$$w_{i,n} = \frac{\eta}{\eta + |\nabla x_{i,n}| \cdot \|p_{i,n}\|_2}. \quad (12)$$

The values of $w_{i,n}$ range between 0 and 1, and they are inversely proportional to $|\nabla x_{i,n}|$. Small gradients will have a larger regularization weight (close to 1), and as a result these small gradients will tend to be shrunk towards 0 in 11. However, point-wise reweighting does not have the capacity to separate geometrically salient structures, such as edges or isolated singularities, from textured regions. Proposition 3.1 showed that isolated gradients, corresponding to those salient geometric features, provide better identifiability than regions with dense large gradients. In order to perform this geometric detection, it is thus necessary to consider non point-wise weights. 12 considers the local ℓ_2 norm $\|p_{i,n}\|_2$ over a neighbourhood at each given location. Isolated features have large local energy relative to non-sparse, textured regions. Therefore, $w_{i,n}$ will tend to attenuate those textured regions in favour of salient geometry. In our experiments, we set patch size $R = 5$ and $\eta = \|\nabla y - \nabla x_n \star k_n\|^2$ to progressively anneal the offset in 12.

Our k -update step uses a sparsity promoting ℓ_p norm $\lambda \|k\|_{0.5}$ with $\lambda = 6 \cdot 10^{-3}$. We also introduce a novel reweighted ridge regression prior on the kernel. The standard unweighted ridge regression term $\|k\|_2^2$ acts uniformly on all frequencies of the kernel k , since $\|k\|^2 = \|\mathcal{F}k\|^2 = \sum_{\omega} |k_f(\omega)|^2$, where $k_f \equiv \mathcal{F}k$. We change this to a *frequency dependent* weighting $\sum_{\omega} \alpha_{\omega} |k_f(\omega)|^2$. The positive weights α_{ω} are chosen to counteract the effect of aperture in the blurring process.

When a certain frequency of the observation $y_f(\omega)$ has very little energy, there is a fundamental ambiguity: is $|y_f(\omega)|$ small because $|x_f(\omega)|$ was near-zero (aperture) or was there a near-zero in the frequency of the kernel $k_f(\omega)$ that attenuated the energy in $\hat{x}(\omega)$? Hence at such ambiguous frequencies, we increase regularization strength. On other frequencies with significant energy, we reduce the regularization strength. We therefore choose the weights α_{ω} to be inversely proportional to the observation energy, as follows:

$$\alpha_{\omega} = \frac{\lambda_{ap}}{1 + |y_f(\omega)|} \quad (13)$$

where λ_{ap} is set to 200 for all experiments reported in this paper. Note that we are using the Fourier transform of the observed image y and not the Fourier transform of ∇y . A constant of 1 was empirically added to the denominator to give a certain minimal level of regularization for robustness to noise and to move away from the trivial δ kernel. The matrix A given in 11 above is therefore simply a product of

a diagonal matrix with the appropriate Fourier matrix. The diagonal entries of the diagonal matrix are given by $\sqrt{\alpha_\omega}$.

We solve the x update step in (11) by performing 30 iterations of Conjugate Gradient with a fixed value of weights $w_{i,n}$, which achieves high accuracy owing to its quadratic formulation. The kernel update in (11) is solved using IRLS. After every k update, we set negative elements of k to 0, and normalize the sum of the elements to 1. We embed the entire framework in a multi-scale framework and perform 20 alternating iterations of x and k at each level. The weights $w_{i,n}$ are updated after every alternating iteration. The weights α_ω and the matrix A are computed once at the beginning and do not change during the iterations.

5 Experimental Results

In this section, we compare our algorithm to that of Cho and Lee [2], Levin et al. [6], and Xu et al. [9]. Our algorithm parameters are fixed to the values given in 4.

We start with the test dataset of [17]. This consists of 4 images blurred with 8 motion blur kernels, giving rise to 32 blurred image-kernel pairs. The standard method of comparison is to compute the ratio of the mean square error of the recovered image with the mean square error of the blurred image deconvolved with the ground-truth kernel, which is known. For all comparisons in this section, we use the sparsity based non-blind deconvolution method of Levin et al. [6] to perform the final non-blind deconvolution step. We use the executable downloaded from the website of the authors of [9] and used existing results for [2] (provided with the code of [6]). We used the same non-blind deconvolution technique provided with the code of [17] with the same parameter settings.

Error ratios less than 3 are considered visually good. 2 shows the cumulative error ratios and our recovered kernels for the different images. It is seen that our algorithm outperforms the other methods, with 90% of the images achieving an error ratio less than 2. However, all the algorithms perform quite well. This is to be expected since each of these methods does promote sparsity of the gradients. The kernels we recover, are very close to the ground-truth kernels shown in the last row. Using patches of size $R = 5$ in 12 performed better than using $R = 1$ i.e. point wise estimation. This is not surprising as isolated gradients can be better detected with larger patch sizes.

The effect of the new kernel prior (11) is especially obvious in the fourth image from the dataset of [17]. This image consists of most gradients oriented in a particular direction and very few in other directions. This leads to poor estimation for frequencies that are orthogonal to the dominant frequencies. The use of an isotropically weighted kernel ℓ_2 prior leads to either an excessively diffuse kernel in

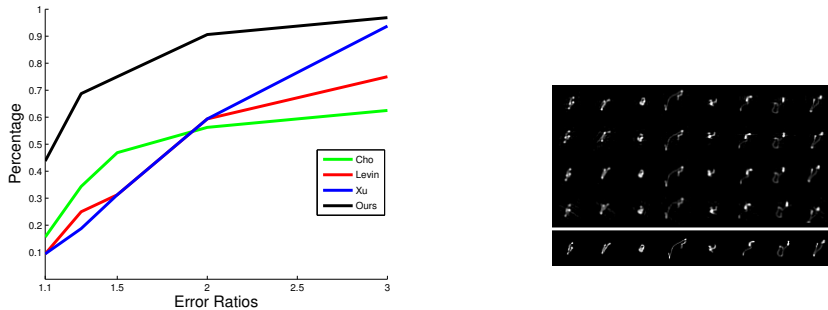


Figure 2: Left: Performance on dataset of Levin et al. [17]. We compare the following methods: the variational algorithm of Levin et al. [6]; the *MAP* algorithms of Cho and Lee [2] and Xu et al. [9]; and our new algorithm. Our algorithm is the top-performing. Right: our recovered kernels are shown: the top 4 rows correspond to the 4 images and the 8 columns correspond to the kernels we recover for each image. The last row shows the 8 ground truth kernels.

low energy directions or an excessively sparse kernel in all directions, depending on the regularization strength. In fact, this artifact is visually visible in the results of both Xu et al. [9] and Levin et al. [6], since they use an isotropically weighted ℓ_2 prior. Numerically as well, the errors are higher for this image. In our results in 2, the kernels on the fourth row are visually and numerically nearly as accurately recovered, as for the other rows.

Next, we compare with some real-world examples. In 3, we compare methods on an example from Xu et al. [9] (distributed as part of their software package). We show here the output of the executable of [9], which appears somewhat inferior to the result in their paper (nevertheless still being quite good).

In 4, we use an image from Goldstein and Fattal [4]. The algorithm in that paper is based on spectral arguments, and so does not fall under the variational or *MAP* categories. Our method, Cho and Lee [2] and Xu et al. [9] perform well. The output of Levin et al. [6] results has artifacts around the edges.

In a recent paper, Lin et al. [19] proposed a new algorithm to handle deblurring in the case of very high noise levels. We show that our proposed algorithm is quite robust to such situations by using an example from their paper (5). The algorithm of Xu et al. [9] produces significant ringing. These could possibly be reduced by parameter adjustments, but no parameters are exposed in their executable. Note that unlike the conclusions of Lin et al. [19], we find that the algorithm of Levin et al. [6] works quite well on this example.

The code of Wipf and Zhang [10] is not available. However, we note that our method seems to perform as well as theirs on the dataset of Levin et al. [17]. Finally,

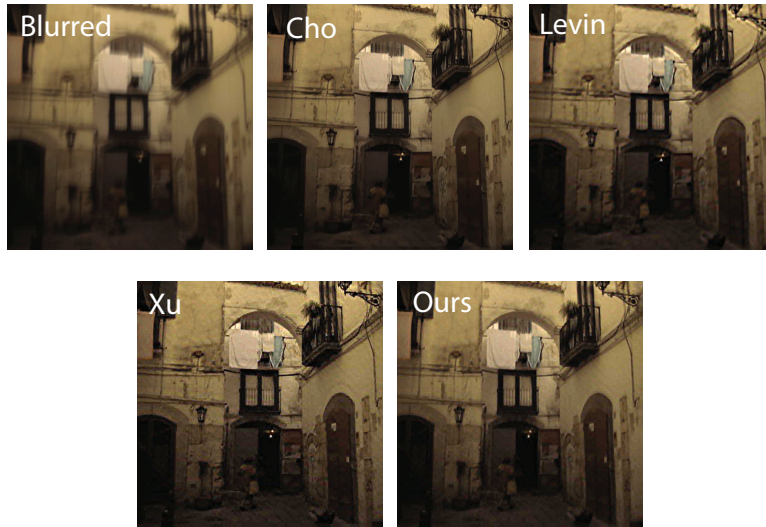


Figure 3: A real-world example from Xu et al. [9]. Our method performs as well as that of [9] and Cho and Lee [2]. Levin et al. [6] exhibits some ringing artifacts.

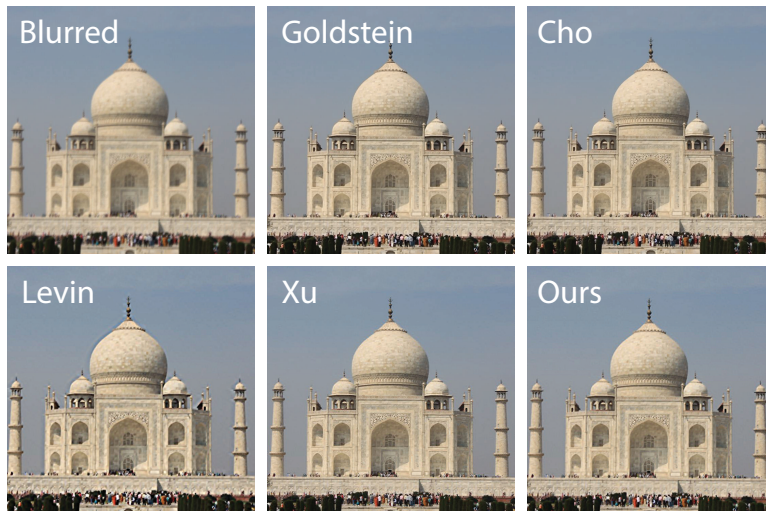


Figure 4: An example from Goldstein and Fattal [4]. We also include their result for comparison.

by modifying the likelihood term using the ideas in Whyte et al. [27], our method can be extended to the case of blur due to camera in-plane rotation. Our code and test data is available at www.xxx.yyy.

6 Discussion

In this paper, we have discussed a number of common properties of successful blind deconvolution algorithms, with sparsity promotion being the most important. In spite of the good performance of existing methods, a number of open problems remain.

The original formulation 1 is non-convex, and alternating minimization schemes are only guaranteed to reach a local minimum. The use of a multi-scale pyramid improves the numerical convergence, but it is quite possible to get stuck in sub-optimal solutions even in that scenario. These problems tend to be exacerbated in large images with many levels in the pyramid, where errors from the coarse to fine scheme may gradually accumulate. Therefore, other minimization strategies such as the convex programming based approach of Ahmed et al. [24] may prove to be better initialization strategies than the multi-scale scheme.

Existing sparsity promoting schemes are not consistent estimators of the blurring kernel k_0 because as the size of the input y increases, they are penalised by estimation errors on the x_0 . Consistent estimators may be obtained by extracting stable geometric structures, using non-local regularisation terms, such as those presented in (12). Highly oscillatory textures do not corrupt the estimation of k_0 , thus showing that sparsity can be highly efficient even when input images do not have sparse gradients. Reweighting schemes provide efficient algorithms for that purpose, although their mathematical properties remain an open issue.

A Proof of Proposition 3.1

Given Ω , we define $\Omega_S = \{i \text{ s.t. } dist(i, \Omega) \leq S\}$, and we decompose the likelihood term as

$$\|y - \tilde{x} \star k\|^2 = \|y - \tilde{x} \star k\|_{\Omega_S}^2 + \|y - \tilde{x} \star k\|_{\Omega_S^c}^2. \quad (14)$$

Since $x|_{\Omega_S^c} \equiv 0$, and k has compact support smaller than S , it results that

$$\|y - \tilde{x} \star k\|^2 = \|y - \tilde{x} \star k\|_{\Omega_S}^2 + \|y\|_{\Omega_S^c}^2,$$

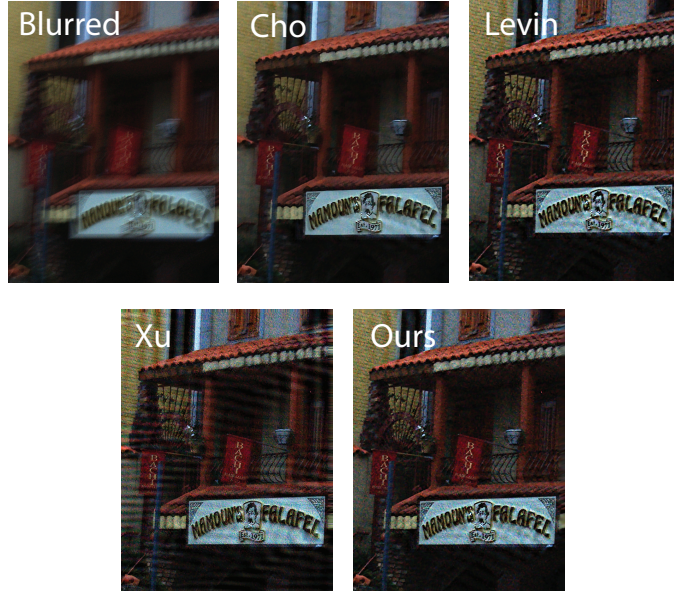


Figure 5: A real-world example from Lin et al. [19] that exhibits blur and high noise levels. Note that unlike [19], we find that the method of Levin et al. [6] also performs well. The results of Xu et al. [9] exhibits significant ringing.

and hence

$$\begin{aligned}
 \hat{k}_0 &= \arg \min_k \|y - \tilde{x} \star k\|^2 + \lambda \|k\|^2 \\
 &= \arg \min_k \|y - \tilde{x} \star k\|_{\Omega_S}^2 + \lambda \|k\|^2 .
 \end{aligned} \tag{15}$$

Since $\sum_i \hat{k}_{0_i} = \sum_i k_{0_i} = 1$ by construction, we shall restrict ourselves to the subspace $\{k; \langle k, \mathbf{1} \rangle = 1\}$. If $y = x_0 \star k_0 + n$ and $e = x_0 - x$, it follows that

$$\hat{k}_0 = \arg \min_k \|x_0 \star (k_0 - k) + n - e \star k\|_{\Omega_S}^2 + \lambda \|k\|^2 .$$

By denoting by A and \tilde{A} the linear operators

$$A(y) = P_{\Omega_S}(x_0 \star y) , \quad \tilde{A}(y) = P_{\Omega_S}(e \star y) ,$$

it results from (15) that

$$\begin{aligned}
 \hat{k}_0 &= \left((A + \tilde{A})^T (A + \tilde{A}) + \lambda \mathbf{I} \right)^{-1} [(A + \tilde{A})^T A k_0 + (A + \tilde{A})^T n] \\
 &= (\bar{A} + F)^{-1} (\bar{A} k_0 + f) ,
 \end{aligned}$$

with $\bar{A} = A^T A$, $F = A^T \tilde{A} + \tilde{A}^T A + \tilde{A}^T \tilde{A} + \lambda \mathbf{I}$ and $f = \tilde{A}^T A k_0 + (A + \tilde{A})^T n$. Since $\delta > 0$, it results that $\bar{A} = A^T A$ is invertible in the subspace of 0-mean vectors. Since

$$(\bar{A} + F)^{-1} (\bar{A} k_0 + f) = (\mathbf{1} + \bar{A}^{-1} F)^{-1} k_0 + \bar{A}^{-1} f ,$$

it follows that

$$\begin{aligned} \|\widehat{k}_0 - k_0\| &\leq \|(\mathbf{I} + \bar{A} F)^{-1} - \mathbf{I}\| \|k_0\| + \delta \|f\| \\ &\leq \frac{\|\bar{A} F\|}{1 - \|\bar{A} F\|} \|k_0\| + \delta^{-1} (\epsilon \|k_0\| \gamma + (\gamma + \epsilon) \|n\|_{\Omega}) \\ &\leq O(\max(\epsilon \delta^{-1/2}, \epsilon \gamma \delta^{-1}, \lambda)) \|k_0\| + O((\gamma + \epsilon) \delta^{-1} \|n\|_{\Omega}) \quad \square . \end{aligned}$$

References

- [1] Fergus, R., Singh, B., Hertzmann, A., Roweis, S.T., Freeman, W.: Removing camera shake from a single photograph. *SIGGRAPH* **25** (2006) 787–794
- [2] Cho, S., Lee, S.: Fast motion deblurring. *SIGGRAPH ASIA* **28**(5) (2009)
- [3] Xu, L., Jia, J.: Two-phase kernel estimation for robust motion deblurring. *ECCV* (2010) 157–170
- [4] Goldstein, A., Fattal, R.: Blur-kernel estimation from spectral irregularities. In: *ECCV*, Springer (2012) 622–635
- [5] Wang, C., Yue, Y., Dong, F., Tao, Y., Ma, X., Clapworthy, G., Lin, H., Ye, X.: Nonedge-specific adaptive scheme for highly robust blind motion deblurring of natural images. *IEEE Trans. on Image* **22**(3) (2013)
- [6] Levin, A., Weiss, Y., Durand, F., Freeman, W.T.: Efficient marginal likelihood optimization in blind deconvolution. In: *CVPR, 2011, IEEE* (2011) 2657–2664
- [7] Whyte, O., Sivic, J., Zisserman, A.: Deblurring shaken and partially saturated images. In: *ICCV Workshops, 2011, IEEE* (2011) 745–752
- [8] Hirsch, M., Schuler, C.J., Harmeling, S., Scholkopf, B.: Fast removal of non-uniform camera shake. In: *ICCV, IEEE* (2011) 463–470
- [9] Xu, L., Zheng, S., Jia, J.: Unnatural L_0 sparse representation for natural image deblurring. In: *CVPR*. (2013)

- [10] Wipf, D., Zhang, H.: Revisiting bayesian blind deconvolution. arXiv:1305.2362 (2013)
- [11] Krishnan, D., Fergus, R.: Fast image deconvolution using hyper-laplacian priors. In: NIPS. (2009)
- [12] Levin, A., Fergus, R., Durand, F., Freeman, W.: Image and depth from a conventional camera with a coded aperture. SIGGRAPH **26**(3) (2007) 70
- [13] Tappen, M.F., Russell, B.C., Freeman, W.T.: Exploiting the sparse derivative prior for super-resolution and image demosaicing. In: SCTV. (2003)
- [14] Levin, A., Weiss, Y.: User assisted separation of reflections from a single image using a sparsity prior. PAMI **29**(9) (Sept 2007) 1647–1654
- [15] Shan, Q., Jia, J., Agarwala, A.: High quality motion deblurring from a single image. SIGGRAPH **27** (2008)
- [16] Cai, J.F., Ji, H., Liu, C., Shen, Z.: Blind motion deblurring from a single image using sparse approximation. In: CVPR, IEEE (2009) 104–111
- [17] Levin, A., Weiss, Y., Durand, F., Freeman, W.T.: Understanding and evaluating blind deconvolution algorithms. In: CVPR. (2009)
- [18] Miskin, J., MacKay, D.J.: Ensemble learning for blind image separation and deconvolution. In: Advances in independent component analysis. Springer (2000) 123–141
- [19] Zhong, L., Cho, S., Metaxas, D., Paris, S., Wang, J.: Handling noise in single image deblurring using directional filters. In: CVPR. (2013)
- [20] Osher, S., Rudin, L.I.: Feature-oriented image enhancement using shock filters. SIAM Journal on Numerical Analysis **27**(4) (1990) 919–940
- [21] Chambolle, A.: An algorithm for total variation minimization and applications. Journal of Mathematical Imaging and Vision **20**(1-2) (2004) 89–97
- [22] Rudin, L., Osher, S., Fatemi, E.: Nonlinear total variation based noise removal algorithms. Physica D **60** (1992) 259–268
- [23] Chan, T.F., Wong, C.K.: Total variation blind deconvolution. IEEE Transactions on Image Processing **7**(3) (1998) 370–375

- [24] Ahmed, A., Recht, B., Romberg, J.: Blind deconvolution using convex programming. arXiv:1211.5608 (2012)
- [25] Daubechies, I., DeVore, R., Fornasier, M., Güntürk, C.S.: Iteratively reweighted least squares minimization for sparse recovery. CPAM **63**(1) (2009) 1–38
- [26] Krishnan, D., Tay, T., Fergus, R.: Blind deconvolution using a normalized sparsity measure. In: CVPR, IEEE (2011) 233–240
- [27] Whyte, O., Sivic, J., Zisserman, A., Ponce, J.: Non-uniform deblurring for shaken images. In: CVPR. (2010)